arXiv:1702.03359v1 [cond-mat.supr-con] 11 Feb 2017

Coexistence between magnetism and superconductivity within the Kondo–attractive-Hubbard model: the borocarbides as a case study.

Natanael C. Costa,[1,*] José Pimentel de Lima,[2] Thereza Paiva,[1]
Mohammed ElMassalami,[1] and Raimundo R. dos Santos[1]

[1] *Instituto de Física, Universidade Federal do Rio de Janeiro, Rio de Janeiro, RJ - Brazil*
[2] *Departamento de Física, Universidade Federal do Piauí, Teresina, PI - Brazil.*

With the purpose of investigating coexistence between magnetic order and superconductivity, we consider a model in which conduction electrons interact with each other, via an attractive Hubbard on-site coupling U, and with local moments on every site, via a Kondo-like coupling, J. The model is solved on a simple cubic lattice through a Hartree-Fock approximation, within a 'semi-classical' framework which allows spiral magnetic modes to be stabilized. For a fixed electronic density, n_c, the small J region of the ground state ($T = 0$) phase diagram displays spiral antiferromagnetic (SAFM) states for small U. Upon increasing U, a state with coexistence between superconductivity (SC) and SAFM sets in; further increase in U turns the spiral mode into a Néel antiferromagnet. The large J region is a (singlet) Kondo phase. At finite temperatures, and in the region of coexistence, thermal fluctuations suppress the different ordered phases in succession: the SAFM phase at lower temperatures and SC at higher temperatures; also, reentrant behavior is found to be induced by temperature. Comparison with experimental data for the borocarbides family reveals that, when J is properly renormalized by the total angular momentum, the magnetic critical temperature, T_N, scales with dG, the de Gennes factor, in line with the measured behavior. By correlating t/U with the ionic radii, we obtain a very satisfactory description of the trend in magnetic and superconducting phases observed in $R\mathrm{Ni_2B_2C}$, with R running across the magnetic rare earths. And, finally, our model reproduces qualitatively some features of $R(\mathrm{Ni}_{1-x}\mathrm{Co}_x)_2\mathrm{B_2C}$, with R = Ho and Er, namely the suppression of superconductivity for $x \ll 1$, a slowly varying $T_N(x)$, and a region of coexistence between superconductivity and spiral phases.

PACS numbers: 71.27.+a, 71.10.Fd, 75.10.-b, 75.30.Mb

I. INTRODUCTION

Coexistence between magnetic order and superconductivity (SC) has been experimentally observed in many classes of materials, such as high-temperature cuprates,[1,2] pnictides,[2,3] heavy fermions,[4] and quaternary rare-earth compounds, such as the borocarbides.[5–9] One expects that a knowledge of the interactions at play leading to such coexistence could shed some light onto the very nature of the pairing mechanisms in unconventional superconductors. As a step towards this final goal, the quaternary borocarbides (QBC) family of compounds provides a very convenient starting point. Indeed, they are conventional phonon-based superconductors, with the general formula $R\mathrm{T_2B_2C}$, in which R is a rare earth element, and T is a transition metal; the magnetic moments come from the rare earths, and the transition metal specifies the density of conduction electrons.[7] A great deal of experimental data relative to the borocarbides has been gathered over the past decades, including alloying the rare earths or the transition metals (see, e.g., Refs. 7, 9–13, and references therein), with the outcome that many different magnetic modes can be stabilized with, or without, superconductivity.

In spite of the large experimental effort to characterize these materials, only a few issues have been addressed theoretically.[14–24] For instance, Refs. 15 and 16 focused on the behavior of $\mathrm{HoNi_2B_2C}$ in the presence of an external magnetic field; their mean-field results are in qualitative agreement with experimental observations of metamagnetic transitions. References 20–22 similarly concentrate on the magnetic behavior of specific compounds. Therefore there is little room in these approaches to learn about the coexistence and competition between SC and magnetism across the whole QBC families; that is, it would be desirable to set up a simple model which could provide a *global* description of the QBC. Along this path, a considerable degree of systematization in the borocarbides was achieved with the introduction of a layered attractive Hubbard model (LAHM):[23] sites i with on-site pairing potentials, $U_i = U$, are intercalated with free j sites, $U_j = 0$; the former sites mimick the nonmagnetic T_2B_2 layers, and the latter mimick the RC layers. In addition, a band offset ε_i (different site energies, or local chemical potentials) between these layers have the effect of extending pair coherence over the free sites:[23] superconductivity is stable for $\varepsilon \geq \varepsilon_c(U)$, where $\varepsilon_c(U)$ is a U-dependent critical value of the band offset. If one assumes that (1) the magnitude of the attractive potential tracks the Debye temperature, which in turn tracks the inverse ionic radii of the rare earths,[25] and (2) the band offset tracks the transition metals within the same group in the periodic table, then a qualitative phase diagram reproduces the phenomenology of $R\mathrm{T_2B_2C}$ quite nicely,[23] as far as being superconductors or not. Since no localized magnetic moments were included in this layering model, one could not probe coexistence between superconductivity and magnetic ordering. Such coexistence

was later examined in a Kondo-attractive Hubbard model (KAHM),[24] in which every site of a lattice is occupied by a localized spin-1/2 (an *effective* single f-electron), coupled locally to the conduction electron through a Kondo-like exchange term, J; the conduction electrons hop between nearest neighbor sites, and the pairing tendency is provided by a uniform attractive Hubbard-U (see below). At this point one should stress that throughout this paper J is concerned with the interaction between superconductivity and magnetic order, and not with the Abrikosov-Gorkov pair-breaking mechanism.[26] Both the LAHM and the KAHM have so far been investigated only in one-dimension, which is amenable to exact calculations on finite-sized lattices. For the KAHM, in particular, density matrix renormalization group calculations showed that coexistence between spiral magnetic phases and superconductivity can indeed be found in the ground state for a range of parameters. For a fixed value of U, a sequence of magnetic modes is found as J increases, ranging from (AFM-like) spin-density waves up to a FM state, though the latter was not found to coexist with superconductivity for any value of U; see Ref. 24. Interestingly, notwithstanding the one-dimensional geometry, the sequence of magnetic modes is consistent with the ones observed in the non-superconducting borocarbide $Tb(Co_xNi_{1-x})_2B_2C$, as J increases;[11,12] the latter, in turn, tracks the Co concentration x (through the Fermi wavevector k_F). Again, this simple model seems to capture the phenomenology of borocarbides, as far as electron count in alloying the transition metal is concerned.

In view of this, a more stringent test of the KAHM is definitely called for. With this in mind, here we investigate the three-dimensional version of this model within a Hartree-Fock (HF) approximation. Since the transport properties of the QBC are isotropic,[8] we consider a simple cubic lattice. However, the 'semi-classical' implementation[27] we use here introduces the experimentally observed anisotropy in the *magnetic lattice*, in the sense that the local moments display a wavevector-dependent average magnetization; this, in turn, allows spiral magnetic states to be stabilized. This approach has unveiled a multitude of magnetic phases in the Kondo lattice model.[27] We are therefore able to discuss the interplay between magnetic modes and superconductivity both in the ground state and at finite temperatures.

This paper is organized as follows: the model and the method are presented in Sec. II (calculational details are left for the Appendix). Sections III and IV respectively discuss the results in the ground state and at finite temperatures. Comparison with experimental data is made in Sec. V. And, finally, Sec.VI summarizes our findings.

II. MODEL AND METHOD

The Hamiltonian for the Kondo–attractive-Hubbard model[24] can be written as

$$\mathcal{H} = \mathcal{H}_K + \mathcal{H}_U, \tag{1}$$

with

$$\mathcal{H}_K = -t \sum_{\langle i,j\rangle,\sigma} \left(c^\dagger_{i\sigma} c_{j\sigma} + \text{H.c.}\right) + J \sum_i \mathbf{S}_i \cdot \mathbf{s}^c_i \tag{2}$$

and

$$\mathcal{H}_U = -U \sum_i n_{i\uparrow} n_{i\downarrow}, \tag{3}$$

where the sums run over sites of a simple cubic lattice, with $\langle i,j\rangle$ denoting nearest-neighbor sites, $c^\dagger_{i\sigma}$ and $c_{i\sigma}$ create and annihilate an electron on site i with spin σ, H.c. denotes the hermitian conjugate of the previous expression, and $\mathbf{S}_i$ and $\mathbf{s}^c_i$ are the spin operators for the local moments and conduction electrons, respectively. Therefore, $\mathcal{H}_K$ is the Kondo lattice Hamiltonian describing the interplay between delocalization and magnetic ordering (we take the exchange as $J > 0$). The term $\mathcal{H}_U$ corresponds to a local attractive interaction between conduction electrons, with coupling strength $-U < 0$; $n_{i\sigma} = c^\dagger_{i\sigma} c_{i\sigma}$ is the number operator of conduction electrons on site i and spin σ.

Within a Hartree-Fock approximation, we decouple the quartic terms, leading to a quadratic Hamiltonian, with effective fields to be determined self-consistently. To this end, we write the spin operators in a fermionic basis as

$$\mathbf{S}_i = \frac{1}{2} \sum_{\alpha,\beta=\pm} f^\dagger_{i\alpha} \boldsymbol{\sigma}_{\alpha,\beta} f_{i\beta}, \tag{4}$$

and

$$\mathbf{s}^c_i = \frac{1}{2} \sum_{\alpha,\beta=\pm} c^\dagger_{i\alpha} \boldsymbol{\sigma}_{\alpha,\beta} c_{i\beta}, \tag{5}$$

with $\boldsymbol{\sigma}_{\alpha,\beta}$ denoting the elements of the Pauli matrices, and $f^\dagger_{i\sigma}$ ($f_{i\sigma}$) being creation (annihilation) operators for localized electrons.

Following the procedure outlined in the Appendix , the Hamiltonian of Eq. (1), becomes

$$\mathcal{H}_{MF} = \sum_{\mathbf{k}\sigma}(\epsilon_{\mathbf{k}} - \tilde{\mu})\, c^{\dagger}_{\mathbf{k}\sigma} c_{\mathbf{k}\sigma} + \left(\frac{Jm_f}{2} - Um_c\right)\sum_{\mathbf{k}}\left(c^{\dagger}_{\mathbf{k}\uparrow} c_{\mathbf{k}+\mathbf{Q}\downarrow} + \text{H.c.}\right) - \frac{Jm_c}{2}\sum_{\mathbf{k}}\left(f^{\dagger}_{\mathbf{k}\uparrow} f_{\mathbf{k}+\mathbf{Q}\downarrow} + \text{H.c.}\right)$$
$$+ \frac{3}{4}JV\sum_{\mathbf{k}\sigma}\left(c^{\dagger}_{\mathbf{k}\sigma} f_{\mathbf{k}\sigma} + \text{H.c.}\right) + \frac{JV'}{4}\sum_{\mathbf{k}}\left(c^{\dagger}_{\mathbf{k}\uparrow} f_{\mathbf{k}+\mathbf{Q}\downarrow} + c^{\dagger}_{\mathbf{k}+\mathbf{Q}\downarrow} f_{\mathbf{k}\uparrow} + \text{H.c.}\right) + \epsilon_f \sum_{\mathbf{k}\sigma} f^{\dagger}_{\mathbf{k}\sigma} f_{\mathbf{k}\sigma}$$
$$- t\Delta\sum_{\mathbf{k}}\left(c^{\dagger}_{\mathbf{k}\uparrow} c^{\dagger}_{-\mathbf{k}\downarrow} + \text{H.c.}\right) + N\left[\mu n_c - \epsilon_f + Jm_c m_f + \frac{3}{2}JV^2 - \frac{1}{2}JV'^2 + \frac{Un_c^2}{4} + \frac{(t\Delta)^2}{U} - Um_c^2 - \frac{Un_c}{2}\right], \tag{6}$$

where $\tilde{\mu}$ and $\epsilon_{\mathbf{k}} = -2t\big[\cos(k_x)+\cos(k_y)+\cos(k_z)\big]$ are the chemical potential and the dispersion of the bare conduction electrons, respectively, while n_c is their density; the lattice spacing is taken as unity. The localized electrons are dispersionless, with ϵ_f being their renormalized contribution to the energy. In our approach, the hybridization between c and f bands is represented by the effective fields V and V', which are defined through

$$V \equiv \langle V^0_{ic}\rangle = \langle V^{0\,\dagger}_{if}\rangle = \frac{1}{2}\sum_{\alpha,\beta=\pm}\langle c^{\dagger}_{i\alpha}\mathbb{1}_{\alpha,\beta} f_{i\beta}\rangle, \tag{7}$$

referred to as the singlet hybridization, and through the triplet hybridization,

$$\langle \mathbf{V}_{ic}\rangle = \langle \mathbf{V}_{if}{}^{\dagger}\rangle = V'\big[\cos(\mathbf{Q}\cdot\mathbf{R}_i), \sin(\mathbf{Q}\cdot\mathbf{R}_i), 0\big], \tag{8}$$

with

$$\mathbf{V}_{ic} = \mathbf{V}^{\dagger}_{if} = \frac{1}{2}\sum_{\alpha,\beta=\pm} c^{\dagger}_{i\alpha}\boldsymbol{\sigma}_{\alpha,\beta} f_{i\beta}, \tag{9}$$

and

$$\mathbf{Q} = (q_x, q_y, q_z). \tag{10}$$

The magnetic ordering is probed by the wavevector $\mathbf{Q}$ and the amplitudes m_f and m_c (referring to local moments and conduction electrons, respectively), which describe the average magnetizations,

$$\langle \mathbf{S}_i\rangle = m_f\big[\cos(\mathbf{Q}\cdot\mathbf{R}_i), \sin(\mathbf{Q}\cdot\mathbf{R}_i), 0\big] \tag{11}$$

and

$$\langle \mathbf{s}^c_i\rangle = -m_c\big[\cos(\mathbf{Q}\cdot\mathbf{R}_i), \sin(\mathbf{Q}\cdot\mathbf{R}_i), 0\big], \tag{12}$$

where $\mathbf{R}_i$ is the vector position of site i on the lattice. At this point we note that while the lattice we consider here is *structurally* three-dimensional (cubic), the above *ansatze* for the magnetic degrees of freedom introduce an anisotropy in the *magnetic lattice.*

And, finally, Δ is the (dimensionless) s-wave superconducting order parameter,

$$\Delta = \frac{U}{t}\langle c^{\dagger}_{i\uparrow} c^{\dagger}_{i\downarrow}\rangle = \frac{U}{t}\langle c_{i\downarrow} c_{i\uparrow}\rangle. \tag{13}$$

We note that the local attractive interaction favors on-site pairing,[28,29] so we do not examine other superconducting possibilities such as inter-orbital pairing, e.g., $c^{\dagger} f^{\dagger}$.

The effective fields provided by the mean-field approximation are $\tilde{\mu}$, ϵ_f, V, V', m_f, m_c, $\mathbf{Q}$ and Δ. Actually, $\tilde{\mu}$ and ϵ_f are effective fields included as Lagrange multipliers, in order to fix (in average) the electronic density and the number of local moments per site. The mean-field Hamiltonian can now be diagonalized using Nambu spinor representations, with eight-component spinors, leading to a two-fold degenerated bands $E^n_{\mathbf{k}}$, $(n = 1, \ldots, 8)$. Then, the Helmholtz free energy is

$$F = -\frac{1}{\beta}\sum_{n,\mathbf{k}}\ln\left(1 + e^{-\beta E^n_{\mathbf{k}}}\right) + const, \tag{14}$$

where $\beta = 1/k_B T$.

Minimizing the Helmholtz free energy

$$\left\langle\frac{\partial F}{\partial\tilde{\mu}}\right\rangle = \left\langle\frac{\partial F}{\partial\epsilon_f}\right\rangle = \left\langle\frac{\partial F}{\partial V}\right\rangle = \left\langle\frac{\partial F}{\partial V'}\right\rangle =$$
$$\left\langle\frac{\partial F}{\partial m_f}\right\rangle = \left\langle\frac{\partial F}{\partial m_c}\right\rangle = \left\langle\frac{\partial F}{\partial q_\alpha}\right\rangle = \left\langle\frac{\partial F}{\partial\Delta}\right\rangle = 0, \tag{15}$$

we are able to determined self-consistently the effective fields. The resulting nonlinear coupled equations are solved numerically using standard library routine packages, with aid of the Hellmann-Feynman theorem. One should have in mind that it is the combination of the hybridization terms, (7) and (9), of the semi-classical *ansatze*, (11) and (12), and with the minimization also with respect to $\mathbf{Q}$, that allows the description of spiral phases, as verified in the context of the Kondo lattice model.[27]

III. GROUND STATE PROPERTIES

When $U = 0$, the Hamiltonian reduces to the Kondo lattice model (KLM), which is known to be an insulator at half filling for all J, with a Néel ground state for $J/t < (J/t)_c \approx 4$, and a spin singlet for $J/t > (J/t)_c$.[30]

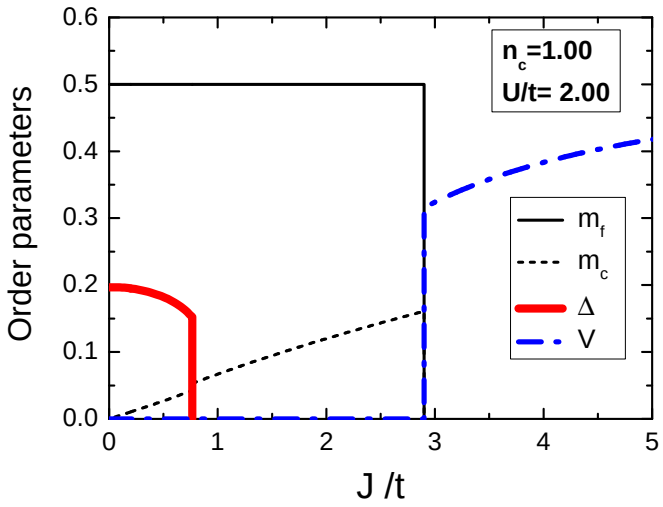

FIG. 1. (Color online) Order parameters (see text for definitions) as functions of J/t, for fixed $U/t = 2$ and at half filling. The magnetic wavevector $\mathbf{Q} = (\pi, \pi, \pi)$ minimizes the free energy for all values of J/t.

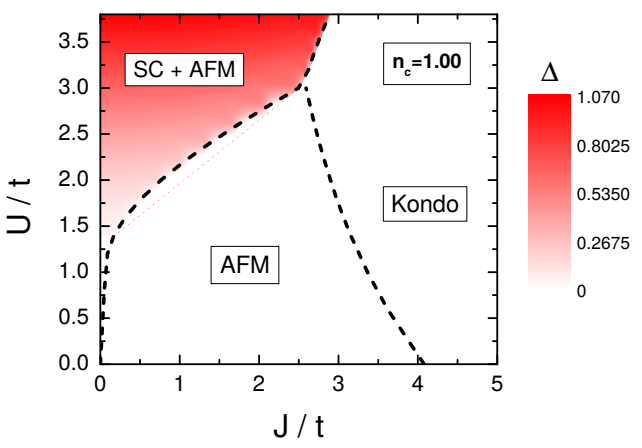

FIG. 2. (Color online) Ground state phase diagram at half filling, showing the antiferromagnetic (AFM), Kondo, and coexisting superconducting and AFM phases (SC+AFM). The dashed lines represent first order phase transitions, while the magnitude of the superconducting gap, Δ, is mapped by the intensity of the shading in the SC+AFM region, with the numerical scale shown to the right of the plotting area. Throughout this paper we adopt the following convention when discussing phase diagrams: continuous and dashed lines respectively denote continuous and first order transitions.

Away from half filling, the system is metallic and spiral states may be stabilized, as recently reported for the two-dimensional case;[27] we will see below that indications of similar sequences of spiral phases are also found in the present three-dimensional case, though we have not pursued here an analysis as detailed as that of Ref. 27. The strong-coupling limit, $J/t \gg 1$, corresponds to the Kondo phase, with conduction electrons strongly hybridized with local moments, thus forming singlets. In the opposite limit, $J = 0$, Eq. (1) reduces to the attractive Hubbard model whose ground state is superconducting for any $U > 0$ and any band filling.[28,31] When both J and U are non-zero, these two tendencies compete with each other, and numerical solutions to the nonlinear coupled equations, Eqs. (15), are sought for a given set of control parameters, (n_c, J, U), with $T = 0$.

Let us first discuss the case of a half-filled conduction band, $n_c = 1$, in which both the AFM and Kondo phases are insulating; in what follows, all borders around the SC+AFM phase correspond to superconductor-insulator phase transitions. Figure 1 shows the different order parameters as functions of J/t, for $U/t = 2$ and at half filling. The superconducting order parameter, Δ, decreases with J/t and vanishes abruptly at $(J/t)_{c1} \approx 0.8$. The magnetization of the localized spins corresponds to $\mathbf{Q} = (\pi, \pi, \pi)$, and its magnitude, m_f, is not affected by the exchange coupling as long as $J/t < (J/t)_{c2} \approx 2.9$, when it drops abruptly to zero. Therefore Néel antiferromagnetism (of the localized spins) coexists with superconductivity up to $(J/t)_{c1}$. Further, the conduction electron magnetization amplitude, m_c, increases with J/t, suffers a tiny burst when superconductivity disappears, and carries on increasing up to $(J/t)_{c2}$, where, similarly to m_f, drops to zero. The picture that emerges is that an increase in J/t leads to a pair-breaking effect followed by an antiferromagnetic coupling of the released electron to the local magnetic moment; for $(J/t)_{c1} < J/t < (J/t)_{c2}$ the pairing tendency disappears, and the Kondo lattice regime of polarized electrons coexisting with the Néel background of local moments remains. Only above $(J/t)_{c2}$ the conduction electrons become hybridized with the local moments (the Kondo phase), thus suppressing magnetic order; at $(J/t)_{c2}$ this is signalled by both the vanishing of m_c and m_f, and the jump of V from zero to a finite value. For completeness, from our experience with the KLM[27] we note that the triplet hybridization only plays some role when there is coexistence between magnetism and the Kondo phase. We have checked that the range of parameters for which this occurs is in fact very narrow in three dimensions, and shrinks even further as $|U|$ increases; for instance, for $n_c = 0.9$ and $3 < J/t < 4$ the AFM+Kondo phase disappears already for $U/t \approx 0.44$.

By performing the same analysis for other values of U, we obtain the phase diagram shown in Fig. 2. Note that $(J/t)_{c1}$ increases with U, while $(J/t)_{c2}$ decreases with U; that is, the purely insulating AFM region shrinks with increasing U, concomitant with an increase in both the coexisting region and the Kondo phase, so that beyond $U/t \approx 3$ the system cannot sustain pure antiferromagnetic order: it is either an antiferromagnetic superconductor or a Kondo insulator, depending on J/t. Figure 2 also indicates that at half filling U cannot change the magnetic mode into a spiral state.

Away from half filling the system behaves quite dif-

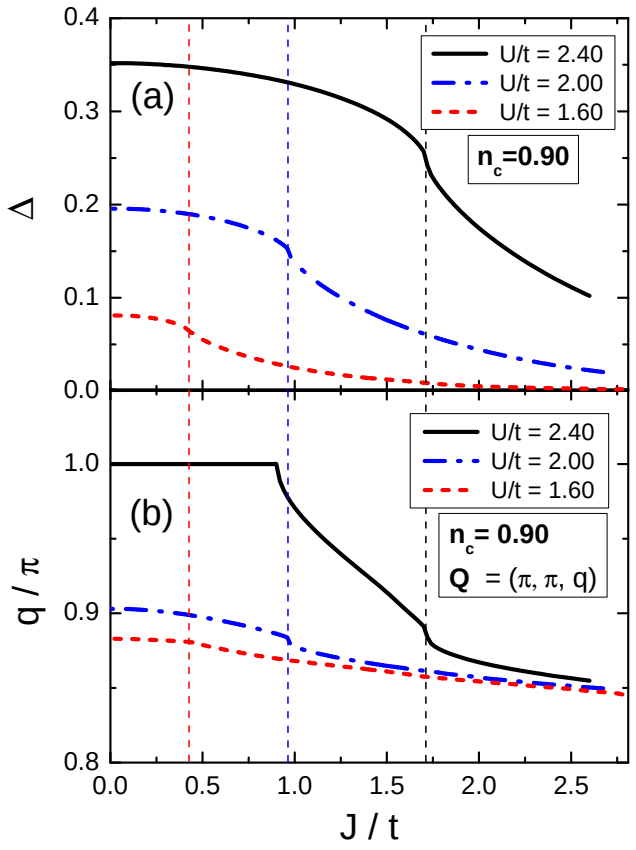

FIG. 3. (Color online) Superconducting gap (a) and z-component of the magnetic wavevector (b) as functions of the Kondo exchange coupling J/t, for three different values of the local attraction U/t. The vertical dashed lines locate the inflection points $(J/t)^{\times}$ for each value of U/t in panel (a), and are prolonged into panel (b) to correlate with the inflections in q; see text.

ferently, as illustrated in Fig. 3(a) for the small doping regime, $n_c = 0.90$, and for three different values of U/t. While increasing J/t is still detrimental to superconductivity, as signalled by the decrease in Δ, here the superconducting gap does not drop to zero abruptly: beyond some inflection point, $J^{\times}(U)$, the gap decays to zero with an exponential tail; from now on, we will refer to this regime as 'weakly superconducting' (WSC),[32] but, as Fig. 3(a) shows, this change in behavior is to be regarded as a crossover, not as a phase transition. This exponential behavior can be attributed to the fact that the superconducting gap for the attractive Hubbard model is expected to behave as[28]

$$\widetilde{\Delta} \simeq W \exp\left(-\frac{1}{N_0 U}\right), \tag{16}$$

where $\widetilde{\Delta}$ denotes the gap in energy units, W is the band width (recall that in standard BCS theory the scale for the gap is set by the Debye energy, $\hbar\omega_D$), and N_0 is the density of states at the Fermi energy in the normal phase.

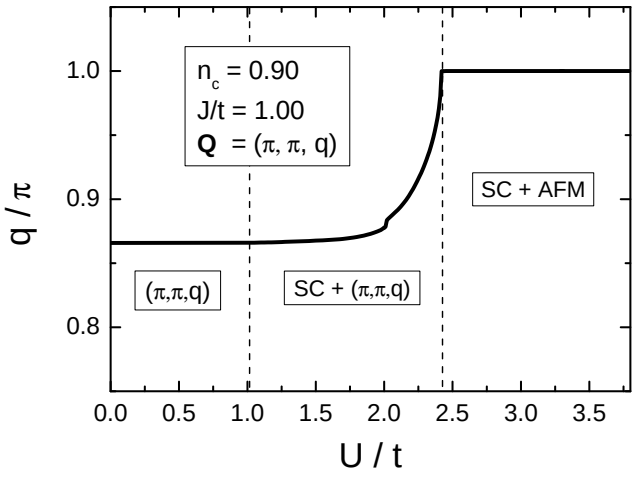

FIG. 4. z-component of the magnetic wavevector as a function of U/t, for a fixed J/t, and away from half filling. The dashed vertical lines indicate change in regimes, for the choice of parameters shown: superconductivity only sets in for $U/t \geq 1$, and the AFM mode is only stable for $U/t \gtrsim 2.4$

Away from half filling the normal state is metallic, so N_0 is finite. Further, an examination of the band structure for the KLM (not shown) reveals that N_0 decreases with increasing J/t, a trend which should also hold for a fixed nonzero U; the gap therefore decreases exponentially with J/t. This argument also explains why the gap vanishes abruptly at half filling: the normal phase is insulating, so that $N_0 = 0$ by decreasing J/t from either the Kondo- or the AFM phases. Figure 3(b) shows the behavior of the magnetic wavevector [actually, of the z-component in $\mathbf{Q} = (\pi, \pi, q)$] with the Kondo coupling: for a fixed U/t, q decreases with J/t, and displays an inflection at the same $(J/t)^{\times}$ as Δ does. It should also be noted that increasing J/t causes q to approach the same finite value, independent of U/t, just before the system enters the Kondo phase. This seems to indicate that before forming singlets, the local moments lock into a magnetic mode which (in the ground state) depends solely on the density of conduction electrons.

From Fig. 3(b) we also see that increasing U/t with fixed J/t has the opposite effect, namely to increase q. Figure 4 provides a closer look at the evolution of q across the different regimes. We note that when the system is either in the normal or WSC regimes, the U dependence of the magnetic wavevector is quite feeble; by contrast, when the system is in the SC regime, the increasing pairing interaction causes a rapid increase in q towards $q = \pi$, thus leading to Néel magnetism coexisting with superconductivity. This can be understood as due to a stronger binding of the local pairs, which in turn polarizes the local moments into a Néel state: any spiral magnetic mode would cost more energy to delocalize the bound pairs; the effective outcome is a smaller pair-breaking effect on the conduction electrons.

The phase diagram in Fig. 5 summarizes our results

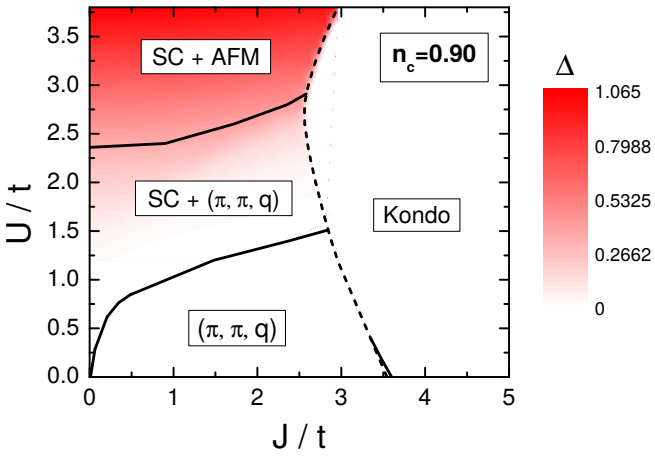

FIG. 5. (Color online) Ground state phase diagram for low doping, $n_c = 0.90$.[25] The magnitude of the superconducting gap, Δ, is mapped by the intensity of the shading in the SC area, with the numerical scale shown to the right of the plotting area. The dependence of q with U/t and J/t is illustrated in Figs. 3 and 4.

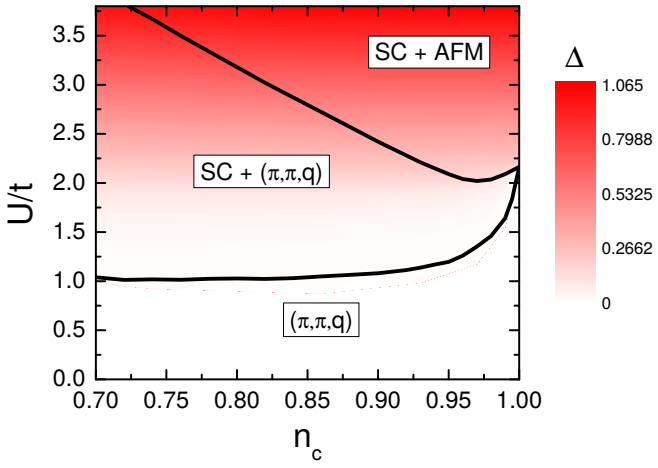

FIG. 6. (Color online) Ground state phase diagram away from half filling, for fixed $J/t = 1.0$. The magnitude of the superconducting gap, Δ, is mapped by the intensity of the shading in the SC+AFM region, with the numerical scale shown to the right of the plotting area.

for $n_c = 0.9$.[33] For small attractive coupling, spiral magnetic order appears without coexistence with SC. However, for larger values of U/t, the ground state displays coexistence between SC and magnetism, with the magnetic wavevector evolving from a spiral mode to AFM, when U/t increases. On the other hand, for large exchange coupling, the Kondo phase is more stable than both SC and magnetism. The trends predicted here are in good agreement with those obtained through DMRG for the same model in one dimension:[24] one of the main features, namely the evolution through incommensurate magnetic modes induced by SC, is also present in our three-dimensional mean-field analysis.

The above analyses are repeated for other electronic densities, and we obtain the phase diagram $U/t \times n_c$, for fixed J/t, displayed in Fig. 6, for $n_c \geq 0.70$. We note that for small U/t, the ground state exhibits a spiral magnetic phase, with $\mathbf{Q} = (\pi, \pi, q)$, which is reminiscent of the KLM, since the attractive potential does not change the magnetic wavevector in the absence of SC, as showed in Fig. 4. When U/t increases, SC sets in and coexistence with magnetism appears. For larger values of U/t the magnetic mode tends to AFM, as discussed before. However, the value of U at which the spiral mode changes to AFM depends quite strongly on the electronic density; the larger the doping, the larger is the value of U/t required to enter the phase SC+AFM. This results from two opposing tendencies. On the one hand, as one dopes the KLM away from half filling, a magnetic mode with $\mathbf{Q} = (\pi, \pi, q)$ changes continuously to $\mathbf{Q} = (\pi, \pi, 0)$;[27] on the other hand, we have seen that increasing U drives the magnetic mode towards $q = \pi$. Therefore, the smaller the electronic density, the larger U must be to induce the $\mathbf{Q} = (\pi, \pi, \pi)$ mode.

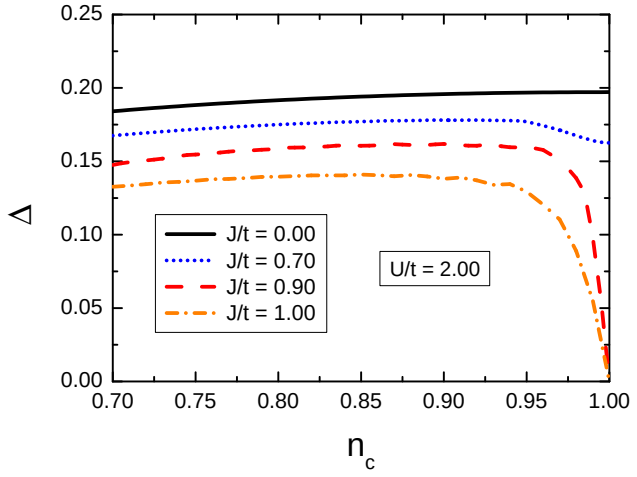

FIG. 7. (Color online) SC order parameter, for fixed $U/t = 2$, as function of the electronic density.

It is also instructive to discuss the behavior of the SC order parameter as a function of n_c for different values of J/t, and fixed U/t, as shown in Fig. 7 for $U/t = 2$; for comparison, the behavior of Δ for the simple attractive Hubbard model ($J/t = 0$) is also shown in Fig. 7. While for $n_c \lesssim 0.9$, the gaps are merely shifted from the AHM case, we note that near half filling the behavior changes significantly with increasing J/t: the SC order parameter is strongly suppressed as half filling is approached. This change in the behavior of Δ occurs abruptly at $J/t \approx 0.75$, which is the transition point where SC is suppressed at half filling, for $U/t = 2$; see Figs. 1 and 2. As we will see in the next Section, this reduction in Δ near half

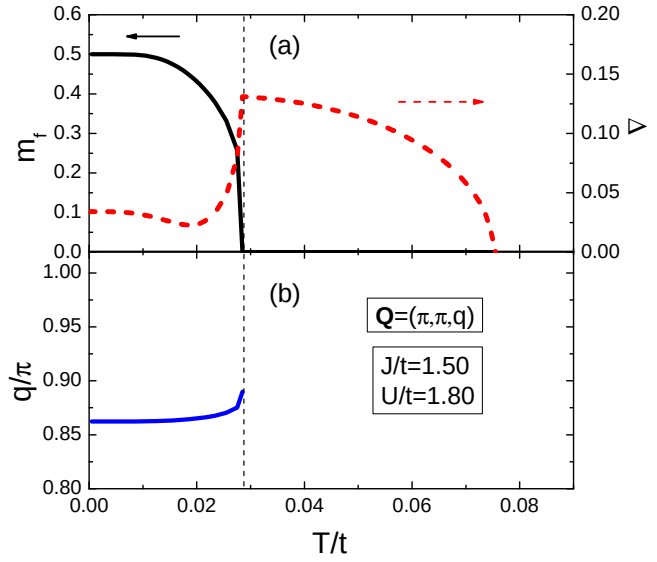

FIG. 8. (Color online) (a) Local moment magnetization amplitude (left vertical scale) and superconducting gap (right vertical scale), and (b) the magnetic wavevector as a function of temperature for fixed $n_c = 0.90$, $J/t = 1.50$ and $U/t = 1.80$.

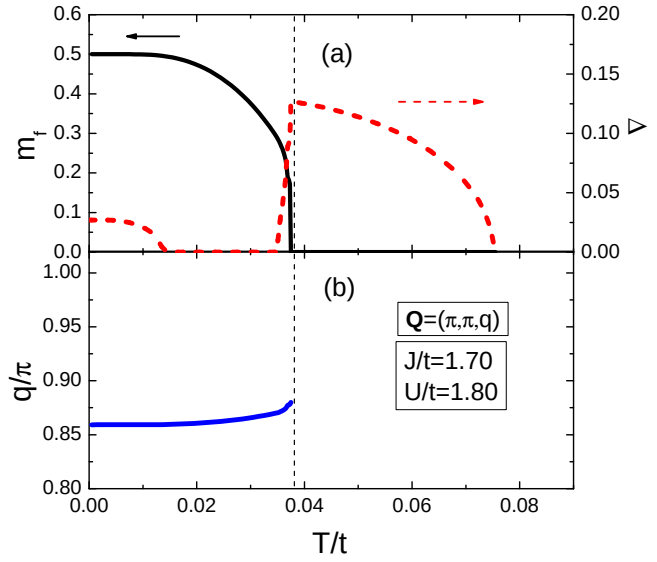

FIG. 9. (Color online) Same as Fig. 8, but for $J/t = 1.70$.

filling leads to a re-entrant-like behavior in SC at finite temperatures.

IV. FINITE TEMPERATURES

We now turn to discuss how the temperature affects the phases observed in the ground state. With the parameter space comprising of temperature, T/t, the couplings J/t and U/t, and the band filling, n_c, we should impose some restrictions on the ranges of J/t and U/t involved,

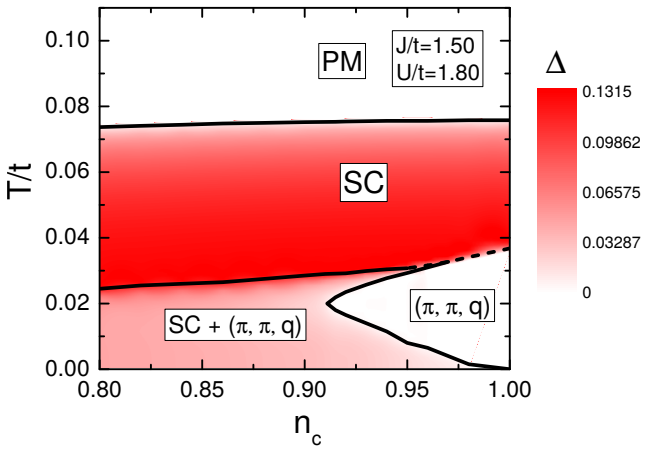

FIG. 10. (Color online) Phase diagram of temperature as function of electronic density for $J/t = 1.5$ and $U/t = 1.8$. The magnitude of the superconducting gap, Δ, is mapped by the intensity of the shading in the SC regions; the numerical scale is shown to the right of the plotting area.

based on some experimental constraints. For instance, for the borocarbides the Néel temperatures,[34] T_N, are of the same order of magnitude as those of the critical temperatures for SC, T_c. We therefore consider ranges of U/t and J/t leading to values for T_N and T_c of similar magnitude; these ranges are narrowed down even further by choosing parameters such that superconductivity coexists with magnetism in the ground state, which, as we have seen, necessarily leads to spiral magnetic modes. As we will see, this suffices to highlight several features arising from the competition between SC and magnetism which become more evident at finite temperatures.

Figure 8(a) shows the dependence of m_f and Δ with the temperature, for fixed $n_c = 0.90$, $J/t = 1.5$ and $U/t = 1.8$. The local-moment magnetization amplitude decreases steadily with the temperature, while the superconducting gap is strongly influenced by the magnetic state. At low temperatures, superconductivity coexists with magnetism, though with a modest gap; when m_f disappears, the gap increases considerably, and the system is purely superconducting until the temperature reaches T_c, at which $\Delta \to 0$. Concerning the magnetic modes, the wavevector is hardly disturbed by the temperature, as shown in Fig. 8(b); only when the temperature approaches T_N, a small increase is noticeable in q.

Increasing J/t favors magnetism, and one expects more pronounced effects in the behavior of the gap with the temperature. Indeed, as displayed in Fig. 9(a), a slight increase in J/t (in comparison with the value used in Fig. 8) results in a complete suppression of Δ within a range of temperatures. However, when $T = T_N$ magnetism disappears, which in turn favors the reemergence of SC. In addition, the behavior of q with T/t depicted in Fig. 9(b) is very similar to that of Fig. 8(b). There-

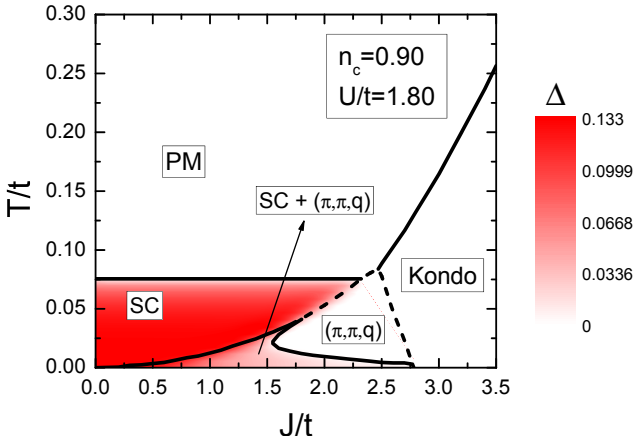

FIG. 11. (Color online) Doniach-like phase diagram for fixed $n_c = 0.90$ and $U/t = 1.8$. The magnitude of the superconducting gap, Δ, is mapped by the intensity of the shading in the SC regions; the numerical scale is shown to the right of the plotting area.

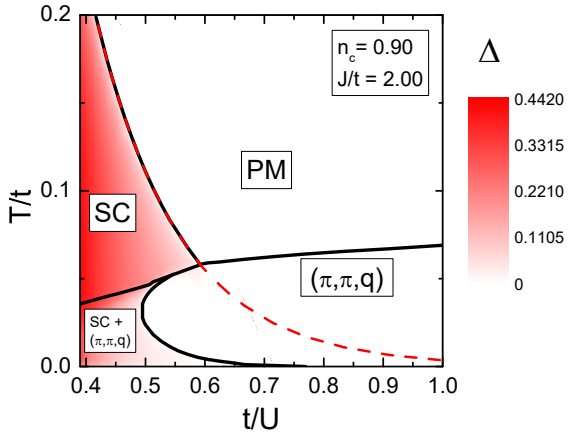

FIG. 12. (Color online) Temperature vs *inverse* on-site attraction, for fixed n_c and J/t. The dashed (red) line is the superconducting critical temperature, T_c, for the attractive Hubbard model (i.e., $J = 0$), which decreases exponentially with t/U, The nearly straight line across the plot is the Néel temperature, T_N. The magnitude of the superconducting gap, Δ, is mapped by the intensity of the shading in the SC regions; the numerical scale is shown to the right of the plotting area.

fore, while magnetism seems to be hardly affected by the coexistence with superconductivity, the converse is not true: the behavior of the SC order parameter is strongly dependent on whether or not there is magnetic order in the background.

By carrying out similar analyses for other fillings while keeping fixed J/t and U/t, we obtain phase diagrams like the one depicted in Fig. 10. For the choice of parameters in the figure, a reentrant superconducting phase is present for $0.91 \lesssim n_c \leq 1$, and one should have in mind that the decrease in the gap depicted in Fig. 8(a) does not configure as a reentrant behavior. We also note that the lobe around the reentrant SC region widens as n_c approaches half filling; this can be attributed to the competition between SC and magnetism in the ground state which, as displayed in Fig. 7, is more detrimental to SC the closer one gets to half filling, and is enhanced as J/t increases. We have explicitly verified (not shown) that as J/t increases, the lobe extends to lower electronic densities, while the boundary between the coexistence region with the purely SC one also rises. Again, this is due to magnetic order being progressively favored as J/t is increased, which increases the temperature interval during which SC is suppressed; also, larger J/t allows the purely magnetic region to be extended to smaller fillings.

Further insight into the main features of the multidimensional phase diagram can be acquired by exploring a $T/t \times J/t$ section for fixed n_c and U/t, such as the one shown in Fig. 11; when $U = 0$ (KLM) this is known as the Doniach phase diagram.[27,35] We note that the coexistence between SC and a spiral phase with $\mathbf{Q} = (\pi, \pi, q)$ is induced as J/t increases. However, the balance is somewhat delicate, since if J/t increases too much one reaches a non-SC spiral phase (also in the shape of a lobe, as in Fig. 10), which eventually leads to a Kondo phase. The boundary at which the spiral phase disappears is the Néel temperature, and it is interesting to see that the RKKY signature of the interaction between local moments, $T_N \propto J^2$, is not modified by the presence of the pairing interaction. Another interesting aspect is that the transition temperature to the (normal) paramagnetic (PM) phase, T_c, is hardly dependent on J/t; the reason for this can be traced back to the fact that once m_f vanishes, ceases the influence of the exchange J/t on the SC state. That is, only the boundaries involving some intervening magnetic ordering are influenced by the exchange coupling.

We now turn to discussing a section $T/t \times U/t$ of the phase diagram, but plotted in terms of t/U, for a more immediate correspondence with experimental data, as discussed in Sec. V. Figure 12 shows data for fixed n_c and J/t. The dashed (red) line is the phase boundary for the $J = 0$ case, highlighting the usual BCS exponential dependence of T_c with t/U, similar to the right-hand side of Eq. (16). The effect of the Kondo coupling is apparent from Fig. 12: First, instead of the exponential decrease of $T_c(U)$ for large t/U, here we see that superconductivity is suppressed more abruptly: it only exists in the ground state up to $t/U_c \approx 0.77$ (see also Fig. 5), and it is also limited to a finite range of t/U at finite temperatures. Second, a spiral magnetic phase emerges at low temperatures, which is completely absent when $J = 0$, and its Néel temperature, $T_N(U)$, increases almost linearly with increasing t/U; also, coexistence between magnetic and superconductor orderings develops at lower temperatures. As noted before, when the spiral phase vanishes

at higher temperatures, the SC-normal boundary is the same as that when $J = 0$. Third, a reentrant SC+spiral phase appears around t/U_c, whose size varies with J/t and n_c. In summary, for given J/t and n_c, superconductivity is suppressed by magnetism for $U \lesssim U_c(n_c, J)$, and by thermal fluctuations [at some $T_c(U, J, n_c)$] when $U \gtrsim U_c(n_c, J)$.

V. COMPARISON WITH EXPERIMENTAL DATA

Due to the diversity in the behavior of the QBC, we concentrate mostly on the $R\mathrm{Ni_2B_2C}$ family of compounds. Within these, we first consider the sequence of the magnetic rare earths, namely R = Tm, Er, Ho, Dy, Tb, and Gd, grouped together according to the de Gennes factor.[6,7,9] We recall that our model considers each local moment as due to a single f-electron, which is coupled to the conduction electrons via an effective exchange coupling, J. In borocarbides, however, each magnetic moment is proportional to the total angular momentum $\mathbf{J}$, including spin and orbital contributions. Then the present exchange J should be replaced by $J\,(g-1)\sqrt{j(j+1)}$, where $j(j+1)$ is the eigenvalue of $\mathbf{J}^2$, and g is the Landé factor. Taking this into account, and for the choice of parameters in Fig. 11, we see that up to $J/t \lesssim 2.5$, the magnetic boundary can be fitted to $T_N \propto J^2(g-1)^2 j(j+1)$, which correctly reproduces the linear scaling of T_N with the de Gennes factor, $dG \equiv (g-1)^2 j(j+1)$, as observed for $R\mathrm{Ni_2B_2C}$, R = Tm, Er, Ho, Dy, Tb, and Gd.[6,7,9]

Reexamining Figures 3 and 5 with the replacement $J \to J \cdot \sqrt{dG}$, we also see that our model additionally reproduces the experimental fact that increasing dG suppresses superconductivity: indeed, the compounds $\mathrm{TbNi_2B_2C}$ and $\mathrm{GdNi_2B_2C}$ (the two with largest dG in the series) order magnetically, but are not superconductors. In addition, Fig. 12 shows that decreasing U in the presence of a fixed J is also deleterious to superconductivity. At this point, the similarity between Figure 12 and Figs. 2 and 4, respectively of Refs. 6 and 7, is to be noted. This suggests that a 'trend-fitting' can be obtained when these heavier rare earths are placed on the horizontal scale, according to their ionic radii. More specifically, R = Tm and Er would lie, in this order, in the region $t/U \lesssim 0.9$ corresponding to $T_c > T_N$.[36] The Ho compound, with $T_c \gtrsim T_N$, displays reentrant superconducting behavior with the temperature; it should therefore be placed in the diagram somewhere in the range $0.5 \leq t/U \lesssim 0.59$. The compound with R = Dy would lie roughly at $t/U \approx 0.6$, corresponding to $T_c < T_N$. Tb and Gd complete the magnetic series, lying in succession in the non-superconducting region, $t/U \gtrsim 0.77$ (the critical value in the ground state). The model also accounts for the appearance of several spiral modes as the coupling constants and temperature are varied; however, attempts to make a close correspondence (through e.g., the de Gennes factor) with the modes observed experimentally[37] as the rare earth changes were not entirely successful. We may attribute this to the lack of layering in the current model; crystal-field effects may also play a role in stabilizing the modes in the observed sequence as the rare earth is varied.[7]

Although this model focuses on the interplay between magnetic order and SC, it is illustrative to see how the remaining QBC fit into this picture. (i) *The non-magnetic and superconducting* R = Lu *and* Y. These compounds have $j = 0$, and their small ionic radii lead to finite values of U/t, so they could be placed in the $J = 0$ section of the full phase diagram. We also note that the compounds with Sc and Th were found to be metastable, though superconducting.[7] (ii) *The magnetic and non-superconducting* R = Sm, Nd, *and* Pr. It has been suggested[7] that rare earth magnetism and strong hybridization between conduction electrons and localized moments may be responsible for the suppression of superconductivity. In the context of our model, both effects can be subsumed by a large value of the Kondo coupling, J/t, and smaller values of U/t; see Figs. 5 and 12. Experimentally, T_N decreases as R goes from Sm to Pr, the opposite tendency displayed in Fig. 12. This illustrates the fact that fixing, say J/t and n_c, and vary solely t/U is only part of the story. In actual fact, changing the rare earth may modify other *effective* parameters of the model; one doesn't follow simple cross sections in the complete phase diagram. In the present case, in going from Tb all the way to Pr, t/U increases, but J/t increases faster, thus causing T_N to increase. (iii) *The mixed valence superconductor* R = Ce,[38] *and the non-magnetic and non-superconducting heavy-fermion* R = Yb. Within our effective model, these features should be associated with a large value of J/t: referring to Fig. 11, the Ce compound would lie in the region $J/t \approx 2.4$, on the verge of Kondo behavior, leading to a very small T_c; the lack of superconductivity for the Yb compound would then be associated with an even larger value of J/t.

The above discussion makes it clear that changing chemical elements, namely R or T, in the QBC formula amounts to simultaneously vary more than one model parameters. To illustrate this point further, we note that the effective exchange coupling J can also be used to track the electron count, since it depends on Fermi surface data, such as k_F and the density of states. It is therefore instructive to compare our theoretical phase diagrams with those obtained by alloying the transition metals in magnetic borocarbides; by choosing transition metals in neighboring columns of the periodic table, and within a rigid-band model, the electronic density is tuned by varying the relative concentration. Indeed, Schmidt and Braun[10] carried out susceptibility and resistivity measurements on $R(\mathrm{Ni}_{1-x}\mathrm{Co}_x)_2\mathrm{B_2C}$, with R = Lu, Tm, Er, Ho, Dy. The overall behavior they found is that the superconducting transition temperature T_c decreases rapidly with increasing x, while the magnetic transition temperature, T_N, is a slowly varying function of x; fea-

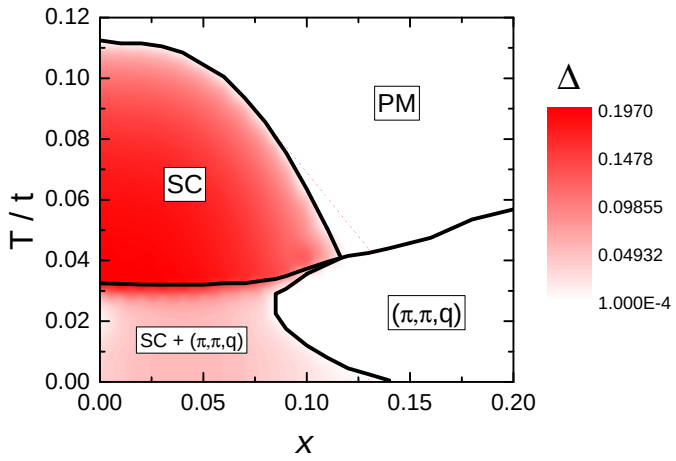

FIG. 13. (Color online) Calculated $T(x)$ phase diagram. The magnitude of the superconducting gap, Δ, is mapped by the intensity of the shading in the SC regions; the numerical scale is shown to the right of the plotting area.

tures such as reentrant behavior have also been found for some specific alloys.[10] In Ref. 10 the authors have also established that alloying can significantly change the magnitude of the electron-phonon coupling constant.

In view of this, the *bare* coupling constants of our model should also incorporate some doping dependence, if one wishes to reproduce the main features of the experimental phase diagrams. With this in mind, we have chosen

$$x = n_c^{(0)} - n_c, \tag{17}$$

$$\tilde{J}/t = J/t + x, \tag{18}$$

$$\widetilde{U}/t = U/t - (\alpha x)^3, \tag{19}$$

as our *effective* parameters, based on the following observations. First, we must stay away from half filling, where the system is an insulator, and the effects of magnetism are particularly detrimental to superconductivity: thus, the reference density is $n_c^{(0)}$, a value close, but not equal, to half-filling, and we also focus on the substitution of Ni by Co, which decreases the number of conduction electrons. Second, the reentrance regions predicted here appear overamplified due to the facts that in the current model, superconductivity and magnetism occur in the same layer. We have found that adjusting $\widetilde{U}$ from the bare U with an x^3 dependence serves the purpose of reducing the reentrance region, while not significantly affecting T_c in the small x region of interest. Accordingly, in the plot displayed in Fig. 13, we have chosen

$$n_c^{(0)} = 0.96, \quad J/t = 1.6, \quad U/t = 2.0, \quad \alpha = 6.5. \tag{20}$$

A comparison between our Fig. 13, and Figs. 8 and 9 of Ref. 10 shows that the main features of the experimental phase diagrams are reproduced by our calculations with the above values. At large doping, superconductivity is suppressed, but a spiral phase persists, while at low doping superconductivity coexists with a spiral phase. The latter phase is only stable up to a magnetic critical temperature, T_N, which, nonetheless, is a slowly varying function of x. Our model therefore reproduces the experimental fact that transition metal substitution affects superconductivity more strongly than magnetism. We should also note that reentrant behavior is present in both experimental diagrams mentioned above (Ref. 10), though still somewhat enlarged in Fig. 13; our data for the behavior of $\mathbf{Q} = (\pi, \pi, q)$ with temperature and other parameters add credence to the suggestion[10] that an abrupt change in the magnetic structure can be at the root of the reentrant behavior.

VI. CONCLUSIONS

We have investigated the issue of coexistence between localized magnetism and superconductivity within an effective microscopic model, comprising of local moments on every site, coupled to conduction electrons by a Kondo-like interaction, J; pairing is made possible by an attractive on-site interaction, U, between the conduction electrons, whose density is n_c. The model is solved on a simple-cubic lattice through a Hartree-Fock approximation within a semi-classical implementation.[27]

We have first mapped out the ground state phases in the parameter space (n_c, J, U). For a fixed band filling, the overall features of the U *vs.* J phase diagrams can be summarized as follows: a Kondo (singlet) phase stabilizes at large J, and magnetic and superconducting phases in the smaller J region; in the latter, as U increases, the purely spiral phase at small U evolves to a phase with superconducting coexisting with spiral antiferromagnetic (SAFM) arrangements (the magnetic wave vector has a weak dependence with U in this phase), and then to a superconducting phase coexisting with a Néel phase. Therefore, the stronger the on-site attraction is, the greater is the tendency towards Néel order in the coexistence phase. Also, at half filling the transition is from a superconducting state to an insulating state, and no spiral phases are stabilized. For completeness, we note that we have not carried out a systematic investigation of the low electronic density region, to map out the boundaries of the ferromagnetic (FM) state, due to the plethora of different magnetic states that emerge in this regime.[27]

Thermal fluctuations also play an important role in suppressing the ordered phases. When the ground state displays coexistence SC+SAFM, increasing the temperature induces two successive transitions: first, the SAFM phase is suppressed, while the SC phase is suppressed at higher temperatures; we note here that the magnetic wave vector shows a weak dependence with the temperature within a phase with SAFM, but it turns stronger just before the SAFM phase is suppressed. When the Kondo phase is the ground state, increasing thermal fluctuations breaks the singlets, and the system becomes paramagnetic at sufficiently high temperatures. Interest-

ingly, in some instances increasing the temperature induces reentrant behavior, namely SC+SAFM → SAFM → SC+SAFM → SC → PM.

Our model reproduces several experimental facts about the borocarbides. First, when the bare exchange coupling J is dressed by the rare earths' total angular momentum, the Néel temperature increases linearly with the de Gennes factor, dG, as observed experimentally. Second, if we correlate the inverse on-site attraction with the ionic radius, we obtain a very satisfactory description of the trend in magnetic and superconducting phases observed in $R\mathrm{Ni_2B_2C}$, with R running across all rare earths; this analysis highlights the difference between model parameters and the 'real' parameters. Third, as an illustration of this, we assume that the main effect of transition metal substitution, as in e.g., $R(\mathrm{Ni}_{1-x}\mathrm{Co}_x)_2\mathrm{B_2C}$, with R = Ho and Er, is to change the electron count in such a way that both J and U acquire a dependence with x. Then, we reproduce the suppression of superconductivity for $x \ll 1$, a slowly varying $T_N(x)$, and a region of coexistence between superconductivity and spiral phases. The multitude of spiral magnetic phases we found by varying electron count and coupling constants is also a trademark of the borocarbides family.

In conclusion, the results highlighted above indicate that the current model contains the main ingredients to capture the diversity of behaviors of the borocarbides family of compounds. Certainly there are physical ingredients which have not been considered here, such as layering and crystalline electric fields; nonetheless, the qualitative agreement between our results and the wealth of experimental data for the phase diagrams indicates that this model already provides a global description of the QBC.

ACKNOWLEDGMENTS

The authors are grateful to the Brazilian Agencies CAPES, CNPq and FAPERJ for financial support.

Appendix: Mean-field approximation

The Hartree-Fock approximation on the attractive potential term, Eq. (3), leads to

$$\mathcal{H}_{U_{(MF)}} = \sum_i \Big[-U\frac{n_c}{2}\big(c^\dagger_{i\uparrow}c_{i\uparrow} + c^\dagger_{i\downarrow}c_{i\downarrow}\big) + \frac{Un_c^2}{4} - t\Delta\big(c^\dagger_{i\uparrow}c^\dagger_{i\downarrow} + c_{i\downarrow}c_{i\uparrow}\big) + \frac{(t\Delta)^2}{U} + 2U\langle \mathbf{s}^c_i\rangle\cdot\mathbf{s}^c_i - U\langle \mathbf{s}^c_i\rangle\cdot\langle \mathbf{s}^c_i\rangle\Big], \quad \text{(A.1)}$$

with

$$\frac{t\Delta}{U} = \langle c^\dagger_{i\uparrow}c^\dagger_{i\downarrow}\rangle = \langle c_{i\downarrow}c_{i\uparrow}\rangle, \quad \text{(A.2)}$$

where Δ is the order parameter of superconductivity, and $n_c = \langle c^\dagger_{i\uparrow}c_{i\uparrow} + c^\dagger_{i\downarrow}c_{i\downarrow}\rangle$ is the electronic density of conduction electrons, both taken as homogeneous throughout the sites. The operator $\mathbf{s}^c_i$ is defined in Eq.(5).

Following the procedure presented in Ref. 27, the Kondo lattice term, Eq. (2), can be decoupled as

$$\mathcal{H}_{K_{(MF)}} = -t\sum_{\langle i,j\rangle,\sigma}\big(c^\dagger_{i\sigma}c_{j\sigma} + \text{H.c.}\big) + J\sum_i\big(\mathbf{S}_i\cdot\langle \mathbf{s}^c_i\rangle + \langle \mathbf{S}_i\rangle\cdot\mathbf{s}^c_i\big) + \frac{J}{2}\sum_i\big(\mathbf{V}^c_i\cdot\langle \mathbf{V}^f_i\rangle + \langle \mathbf{V}^c_i\rangle\cdot\mathbf{V}^f_i\big) - \frac{3J}{2}\sum_i\big(V^0_{ic}\langle V^0_{if}\rangle + \langle V^0_{ic}\rangle V^0_{if}\big) - \frac{J}{2}\sum_i\langle \mathbf{V}^c_i\rangle\cdot\langle \mathbf{V}^f_i\rangle + \frac{3J}{2}\sum_i\langle V^0_{ic}\rangle\langle V^0_{if}\rangle - J\sum_i\langle \mathbf{S}_i\rangle\cdot\langle \mathbf{s}^c_i\rangle, \quad \text{(A.3)}$$

with the operators

$$V^0_{ic} = V^{0\,\dagger}_{if} = \frac{1}{2}\sum_{\alpha,\beta=\pm}c^\dagger_{i\alpha}\mathbb{I}_{\alpha,\beta}f_{i\beta}, \quad \text{(A.4)}$$

and

$$\mathbf{V}_{ic} = \mathbf{V}^\dagger_{if} = \frac{1}{2}\sum_{\alpha,\beta=\pm}c^\dagger_{i\alpha}\boldsymbol{\sigma}_{\alpha,\beta}f_{i\beta}, \quad \text{(A.5)}$$

being singlet and triplet hybridization terms, respectively.

Within a spiral magnetic approach, the mean values $\langle \mathbf{S}_i\rangle$ and $\langle \mathbf{s}^c_i\rangle$ are taken as

$$\langle \mathbf{S}_i\rangle = m_f\big[\cos(\mathbf{Q}\cdot\mathbf{R}_i), \sin(\mathbf{Q}\cdot\mathbf{R}_i), 0\big] \quad \text{(A.6)}$$

and

$$\langle \mathbf{s}^c_i\rangle = -m_c\big[\cos(\mathbf{Q}\cdot\mathbf{R}_i), \sin(\mathbf{Q}\cdot\mathbf{R}_i), 0\big], \quad \text{(A.7)}$$

with

$$\mathbf{Q} = (q_x, q_y, q_z) \quad \text{(A.8)}$$

being the magnetic wavevector, and $\mathbf{R}_i$ the position vector of site i on the lattice.

By the same token, the mean values of the hybridization operators are chosen as

$$\langle V^0_{ic}\rangle = \langle V^{0\,\dagger}_{if}\rangle = -V \quad \text{(A.9)}$$

and

$$\langle \mathbf{V}_{ic} \rangle = \langle \mathbf{V}_{if}{}^{\dagger} \rangle = V' \big[\cos\left(\mathbf{Q}\cdot\mathbf{R}_i\right), \sin\left(\mathbf{Q}\cdot\mathbf{R}_i\right), 0 \big]. \tag{A.10}$$

Then, our mean-field Hamiltonian, Eq. (6), is obtained by substituting Eqs. (A.1) and (A.3) in Eq. (1), using Eqs. (A.6), (A.7), (A.9) and (A.10) for the mean values of the spin and hybridization operators, and performing a discrete Fourier transform, with periodic boundary conditions. Such Hamiltonian is two-fold degenerate when written in the spinor Nambu basis

$$\mathbf{\Psi}^{\dagger}_{\mathbf{k}} = \big(c^{\dagger}_{\mathbf{k}\uparrow}, c^{\dagger}_{\mathbf{k}+\mathbf{Q}\downarrow}, f^{\dagger}_{\mathbf{k}\uparrow}, f^{\dagger}_{\mathbf{k}+\mathbf{Q}\downarrow}, c_{-\mathbf{k}\downarrow}, c_{-\mathbf{k}-\mathbf{Q}\uparrow}, f_{-\mathbf{k}\downarrow}, f_{-\mathbf{k}-\mathbf{Q}\uparrow} \big),$$

leading to

$$\mathcal{H}_{MF} = \Psi^{\dagger}_{\mathbf{k}} \hat{H} \Psi_{\mathbf{k}} + const., \tag{A.11}$$

with

$$\hat{H} = \begin{pmatrix}
\epsilon_{\mathbf{k}} - \tilde{\mu} & \frac{1}{2}Jm_f - Um_c & \frac{3}{4}JV & \frac{1}{4}JV' & -t\Delta & 0 & 0 & 0 \\
\frac{1}{2}Jm_f - Um_c & \epsilon_{\mathbf{k}+\mathbf{Q}} - \tilde{\mu} & \frac{1}{4}JV' & \frac{3}{4}JV & 0 & t\Delta & 0 & 0 \\
\frac{3}{4}JV & \frac{1}{4}JV' & \epsilon_f & -\frac{1}{2}Jm_c & 0 & 0 & 0 & 0 \\
\frac{1}{4}JV' & \frac{3}{4}JV & -\frac{1}{2}Jm_c & \epsilon_f & 0 & 0 & 0 & 0 \\
-t\Delta & 0 & 0 & 0 & -(\epsilon_{-\mathbf{k}} - \tilde{\mu}) & -(\frac{1}{2}Jm_f - Um_c) & -\frac{3}{4}JV & -\frac{1}{4}JV' \\
0 & t\Delta & 0 & 0 & -(\frac{1}{2}Jm_f - Um_c) & -(\epsilon_{-\mathbf{k}-\mathbf{Q}} - \tilde{\mu}) & -\frac{1}{4}JV' & -\frac{3}{4}JV \\
0 & 0 & 0 & 0 & -\frac{3}{4}JV & -\frac{1}{4}JV' & -\epsilon_f & \frac{1}{2}Jm_c \\
0 & 0 & 0 & 0 & -\frac{1}{4}JV' & -\frac{3}{4}JV & \frac{1}{2}Jm_c & -\epsilon_f
\end{pmatrix}. \tag{A.12}$$

and

$$const. = 2N \left[\mu\big(n_c - 1\big) - \epsilon_f \big(n_f - 1\big) + Jm_c m_f + \frac{3}{2}JV^2 - \frac{1}{2}JV'^2 + \frac{Un_c^2}{4} + \frac{(t\Delta)^2}{U} - Um_c^2 - \frac{Un_c}{2} \right]. \tag{A.13}$$

Here, we defined $\tilde{\mu} = \big(\mu - \frac{1}{2}Un_c\big)$, in which μ and ϵ_f are included as Lagrange multipliers.

The eigenvalues of the Hamiltonian of Eq. (A.12) are used to obtain the Helmholtz free energy, Eq. (14), and, consequently, the set of nonlinear equations, Eq. (15).

* natanael@if.ufrj.br

[1] H. Mukuda, S. Shimizu, A. Iyo, and Y. Kitaoka, J. Phys. Soc. Jpn. **81**, 011008 (2012).
[2] D. J. Scalapino, Rev. Mod. Phys. **84**, 1383 (2012).
[3] G. R. Stewart, Rev. Mod. Phys. **83**, 1589 (2011).
[4] C. Pfleiderer, Rev. Mod. Phys. **81**, 1551 (2009).
[5] R. J. Cava, H. Takagi, H. W. Zandbergen, J. J. Krajewski, W. F. Peck Jr., T. Sigerist, B. Batlogg, R. B. Van Dover, R. J. Felder, K. Mizuhashi, J. O. Lee, H. Eisaki, and S. Uchida, Nature **367**, 252 (1994).
[6] P. C. Canfield, P. L. Gammel, and D. J. Bishop, Phys. Today **51**, 40 (1998).
[7] K.-H. Müller and V. N. Narozhnyi, Rep. Prog. Phys. **64**, 943 (2001).
[8] K.-H. Müller, G. Fuchs, S.-L. Drechsler, and V. Narozhnyi, in *Handbook of Magnetic Materials*, Handbook of Magnetic Materials, Vol. 14, edited by K. Buschow (Elsevier, 2002) pp. 199 – 305.
[9] L. C. Gupta, Adv. Phys. **55**, 691 (2006).
[10] H. Schmidt and H. F. Braun, Phys. Rev. B **55**, 8497 (1997).
[11] M. ElMassalami, H. Takeya, B. Ouladdiaf, R. Maia Filho, A. M. Gomes, T. Paiva, and R. R. dos Santos, Phys. Rev. B **85**, 174412 (2012).
[12] M. ElMassalami, A. M. Gomes, T. Paiva, R. R. dos Santos, and H. Takeya, J. Magn. Magn. Mater. **335**, 163 (2013).
[13] M. ElMassalami, H. Takeya, B. Ouladdiaf, A. M. Gomes, T. Paiva, and R. R. dos Santos, J. Magn. Magn. Mater. **372**, 74 (2014).
[14] W. E. Pickett and D. J. Singh, Phys. Rev. Lett. **72**, 3702 (1994).

[15] A. Amici and P. Thalmeier, Phys. Rev. B **57**, 10684 (1998).
[16] A. Amici, P. Thalmeier, and P. Fulde, Phys. Rev. Lett. **84**, 1800 (2000).
[17] H. Ghosh, S. Sil, and S. Behera, Physica C: Superconductivity **316**, 34 (1999).
[18] M. Diviš, K. Schwarz, P. Blaha, G. Hilscher, H. Michor, and S. Khmelevskyi, Phys. Rev. B **62**, 6774 (2000).
[19] Q. Yuan and P. Thalmeier, Phys. Rev. B **68**, 174501 (2003).
[20] V. A. Kalatsky and V. L. Pokrovsky, Phys. Rev. B **57**, 5485 (1998).
[21] J. Jensen, Phys. Rev. B **65**, 140514 (2002).
[22] M. B. Walker and C. Detlefs, Phys. Rev. B **67**, 132407 (2003).
[23] T. Paiva, M. E. Massalami, and R. R. dos Santos, Journal of Physics: Condensed Matter **15**, 7917 (2003).
[24] P. R. Bertussi, A. L. Malvezzi, T. Paiva, and R. R. dos Santos, Phys. Rev. B **79**, 220513 (2009).
[25] Note that the horizontal axis of Fig. 4 in Ref. 23 should read $|U|^{-1}$ instead of $|U|$.
[26] A. A. Abrikosov and L. P. Gor'kov, Sov. Phys. – JETP **12**, 1243 (1961).
[27] N. Costa, J. Lima, and R. R. dos Santos, J. Magn. Magn. Mater. **423**, 74 (2017).
[28] R. Micnas, J. Ranninger, and S. Robaszkiewicz, Rev. Mod. Phys. **62**, 113 (1990).
[29] T. Paiva, R. R. dos Santos, R. T. Scalettar, and P. J. H. Denteneer, Phys. Rev. B **69**, 184501 (2004).
[30] C. Lacroix and M. Cyrot, Phys. Rev. B **20**, 1969 (1979).
[31] R. R. dos Santos, Phys. Rev. B **50**, 635 (1994).
[32] The meaning of *weakly superconducting* in the context of this paper has no connection with the more common usage of the term, denoting the type of superconductivity occurring on a surface or a grain boundary; here it simply denotes a weakening of the gap.
[33] We recall that the phase boundaries are determined by crossings in the lowest ground state energy, and they coincide with those obtained by the vanishing of the different order parameters; when approaching the spiral magnetic phase at small U/t, we observe Δ being smaller than a given tolerance, in accordance with the decreasing exponential behavior.
[34] Here we use the term Néel temperature, T_N, in a broader sense, encompassing the critical temperature for spiral states as well.
[35] S. Doniach, Physica B+C **91**, 231 (1977).
[36] This is intended to be a nothing but a *qualitative* 'fitting' to data; therefore, no quantitative prediction for any of the model parameters should be inferred.
[37] J. W. Lynn, S. Skanthakumar, Q. Huang, S. K. Sinha, Z. Hossain, L. C. Gupta, R. Nagarajan, and C. Godart, Phys. Rev. B **55**, 6584 (1997).
[38] M. ElMassalami, R. Rapp, and G. Nieuwenhuys, Physica C: Superconductivity **304**, 184 (1998).